Available online at www.sciencedirect.com

SciVerse ScienceDirect

Ceramics International 39 (2013) 4847–4851

CERAMICS INTERNATIONAL

www.elsevier.com/locate/ceramint

Influence of doping with various cations on electrical conductivity of apatite-type neodymium silicates

Jun Xiang, Zhan-Guo Liu, Jia-Hu Ouyang*, Yu Zhou, Fu-Yao Yan

School of Materials Science and Engineering, Harbin Institute of Technology, 92 West Da-Zhi Street, Harbin 150001, China

Received 10 October 2012; received in revised form 23 November 2012; accepted 23 November 2012
Available online 1 December 2012

Abstract

Apatite-type neodymium silicates doped with various cations at the Si site, $Nd_{10}Si_5BO_{27-\delta}$ (B=Mg, Al, Fe, Si), were synthesized via the high-temperature solid state reaction process. X-ray diffraction and complex impedance analysis were used to investigate the microstructure and electrical properties of $Nd_{10}Si_5BO_{27-\delta}$ ceramics. All $Nd_{10}Si_5BO_{27-\delta}$ ceramics consist of a hexagonal apatite structure with a space group $P63/m$ and a small amount of second phase Nd_2SiO_5. Neodymium silicates doped with Mg^{2+} or Al^{3+} cations at the Si site have an enhanced total conductivity as contrasted with undoped $Nd_{10}Si_6O_{27}$ ceramic at all temperature levels. However, doping with Fe^{3+} cations at the Si site has a little effect on improving the total conductivity above 873 K. The enhanced oxide-ion conductivity in a hexagonal apatite-type structure depends upon the diffusion of interstitial oxide-ion through oxygen vacancies induced by the Mg^{2+} or Al^{3+} substitution to the Si^{4+} site and through the channels between the SiO_4 tetrahedron and Nd^{3+} cations. At 773 K, the highest total conductivity is 4.19×10^{-5} S cm^{-1} for $Nd_{10}Si_5MgO_{26}$ ceramic. At 1073 K, $Nd_{10}Si_5AlO_{26.5}$ silicate has a total conductivity of 1.55×10^{-3} S cm^{-1}, which is two orders of magnitude higher than that of undoped $Nd_{10}Si_6O_{27}$.

Keywords: B. X-ray methods; C. Electrical conductivity; D. Silicate; Solid state reaction

1. Introduction

Yttria-stabilized zirconia (YSZ) has attracted great attention due to its good chemical stability and high oxide-ion conductivity as solid electrolytes of solid oxide fuel cells (SOFCs). Nevertheless, one of the major problems in the development of YSZ electrolyte is its high operating temperature, which may cause some negative consequences [1,2]. In recent years, oxy-apatite-type structure with the general formula of $Ln_{9.33+x}Si_6O_{26+3x/2}$ (Ln = rare-earth elements) has attracted considerable attention as a new class of ideal electrolyte materials due to its promising benefits of low operating temperature down to 773–1073 K, enhanced long-term stability, a wide range of material selection and relatively low processing cost. $Ln_{10}(SiO_4)_6O_3$ (Ln = La, Nd, Sm, Gd, Dy, Y, Ho, Er and Yb) was prepared for the first time by conventional solid reaction [3]. In apatite-type silicates of $Ln_{10}(SiO_4)_6O_3$ (Ln = trivalent rare-earth elements), the structure is built up of isolated SiO_4 tetrahedra with excess oxide-ions, which are confirmed to migrate in the conduction channel by a complex sinusoidal pathway along the c-axis [4]. Higuchi et al. [5,6] studied single crystal growth and oxide-ion conductivity of apatite-type $Nd_{9.33}Si_6O_{26}$ silicates by the floating zone method. From Nakao's study [7], the conductivity of $Nd_{10}Si_6O_{27}$ was lower than that of $La_{10}Si_6O_{27}$ due to the difference in the capacity of excess oxide-ion acceptance. However, Nakayama et al. [3] investigated the ionic conductivity of different lanthanoid silicates, $Ln_{10}(SiO_4)_6O_3$ (Ln = La, Nd, Sm, Gd, Dy, Y, Ho, Er and Yb), and found that the ionic conductivity of $Nd_{10}Si_6O_{27}$ was quite comparable to that of $La_{10}Si_6O_{27}$.

Many cationic substitutions were usually doped at the La site of lanthanum silicates with alkaline-earth metals or rare-earth elements [8] and at the Si site with Ge, Ga, Al [9,10], and some transition metallic elements [11,12]. However, to the best of our knowledge, no studies have been performed to evaluate the influence of doping with Mg^{2+}, Al^{3+} or Fe^{3+} cations at the Si site on electrical

*Corresponding author. Tel./fax: +86 451 86414291.
E-mail address: ouyangjh@hit.edu.cn (J.-H. Ouyang).

0272-8842/$ - see front matter © 2012 Elsevier Ltd and Techna Group S.r.l. All rights reserved.
http://dx.doi.org/10.1016/j.ceramint.2012.11.077

properties of neodymium silicates. Therefore, in the present work, structure and electrical conductivity of $Nd_{10}Si_5BO_{27-\delta}$ (B=Mg, Al, Fe, Si) ceramics synthesized via the solid state reaction were investigated.

2. Experimental procedures

$Nd_{10}Si_5BO_{27-\delta}$ (B=Mg, Al, Fe, Si) ceramics were synthesized by the solid state reaction process. Commercially available Nd_2O_3 (Grirem Advanced Materials Co. Ltd., Beijing, China; purity $\geq$99.9%), SiO_2 (Huijing New Materials Ltd., Shanghai, China; purity $\geq$99.9%), MgO, Al_2O_3 and Fe_2O_3 (Wanjing New Materials Ltd., Hangzhou, China; purity $\geq$99.9%) powders were used as raw materials. In order to achieve complete decarbonation and dehydroxylation, Nd_2O_3 powders were firstly precalcined at 1173 K for 2 h before weighing. The powders in appropriate ratios were mechanically mixed using zirconia milling media in ethanol for 24 h at a speed of 400 rpm, and were then dried at 373 K. The dried powder mixtures were calcined at 1623 K for 10 h, and were then ground by hand with an agate mortar and pestle. Afterwards, the mixed powders were uniaxially pressed into pellets at 20 MPa. The pellets were further compacted by cold isostatic pressing at 200 MPa for 5 min, and were then pressureless-sintered at 1923 K for 10 h in air. Phase identification of sintered ceramics was determined by X-ray diffraction (XRD, Rigaku D/Max 2200VPC, Japan) with Cu Kα radiation. The XRD patterns were recorded in a 2θ range of 10°–70° at a scan rate of 5° min^{-1}.

Electrical property of $Nd_{10}Si_5BO_{27-\delta}$ (B=Mg, Al, Fe, Si) ceramics was investigated by AC impedance with four-probe method using impedance/gain-phase analyzer (Solartron™ SI 1260, UK) combined with electrochemical interface (Solartron™ SI 1287, UK). The wafer specimen used for impedance measurement has a diameter of 8 mm and a thickness of 1 mm. Electrode was daubed with platinum paste on both surfaces of the samples, and was then heated to 1273 K for 2 h in air in order to ensure that the platinum paste contacts the specimen surfaces and eliminates organic components. Measurements were performed in air between 673 and 1173 K with a 50 K interval in the frequency range of 20 Hz–20 MHz. Impedance complex data were analyzed using the Zview 3.2c software. Total conductivity reported in this paper is designated to be the total electrical conductivity including grain and grain-boundary conductivity owing to the difficulty of accurately separating the grain contribution from the grain boundary contribution.

3. Results and discussion

XRD patterns of apatite-type $Nd_{10}Si_5BO_{27-\delta}$ ceramics doped with various cations at the Si site are shown in Fig. 1. Main diffraction peaks of various $Nd_{10}Si_5BO_{27-\delta}$ ceramics are identified to agree with the standard XRD spectrum of $La_{10}Si_6O_{27}$ (JCPDS no. 53-0291), and the Miller indices are also shown in Fig. 1. Clearly, all $Nd_{10}Si_5BO_{27-\delta}$ ceramics consist of a hexagonal apatite structure with a space group $P63/m$ and a small amount of second phase Nd_2SiO_5. Under most of synthesis and sintering conditions, the second phase La_2SiO_5 in lanthanum silicates was also reported in a previous study [13]. Fig. 2 shows the microstructure of $Nd_{10}Si_5BO_{27-\delta}$ (B=Al, Fe, Si) ceramics. Previous studies [14,15] proved that the cations with a large ionic radius would substitute the La site in lanthanum silicate such as rare-earth elements or Ba, Sr and Ca alkaline-earth elements, while the cations with a small ionic radius would substitute the Si site such as Al, Fe, Ga, etc. The ionic radii of Mg^{2+}, Al^{3+}, and Fe^{3+} are all smaller than that of Nd, so these cations would substitute the Si^{4+} site. From Fig. 1, only $Nd_{10}Si_5BO_{27-\delta}$ (B=Mg, Al, Fe, Si) and a small amount of Nd_2SiO_5 phases are found in the spectra, no starting materials of MgO, Al_2O_3 or Fe_2O_3 have been identified in the as-sintered samples. It indicates that the doping content used in this investigation does not cause the presence of any impurities such as MgO, Al_2O_3 or Fe_2O_3 at the grain boundaries. Table 1 shows the lattice parameters of $Nd_{10}Si_5BO_{27-\delta}$ (B=Mg, Al, Fe, Si) ceramics sintered at 1923 K for 10 h. The lattice parameters of $Nd_{10}Si_5BO_{27-\delta}$ (B=Mg, Al, Fe, Si) ceramics are similar to those reported in previous study [3]. Clearly, doping with Mg^{2+} and Al^{3+} to the tetravalent Si^{4+} site in $Nd_{10}Si_5BO_{27-\delta}$ does not cause a distinct change in the cell volume due to similar lattice parameters of a and c as compared to $Nd_{10}Si_6O_{27}$ ceramic. However, doping with Fe^{3+} to the tetravalent Si^{4+} site leads to a significant expansion in the cell volume. The Fe^{3+} substitution on the Si^{4+} site partly expands the SiO_4 tetrahedra, which will reduce the spacing of channels between the SiO_4 tetrahedron and Nd^{3+} cations in the hexagonal apatite structure. The bulk densities of $Nd_{10}Si_5BO_{27-\delta}$ (B=Mg, Al, Fe, Si) ceramics are given in Table 2.

AC impedance spectroscopy ($-Z''$ vs. Z') of $Nd_{10}Si_5BO_{27-\delta}$ (B=Mg, Al, Fe, Si) ceramics is measured as a function of frequency in the temperature range of 673–1173 K in air, which is characterized by the grain and grain boundary conductivity. Typical complex impedance plots of $Nd_{10}Si_5BO_{27-\delta}$ (B=Mg, Al, Fe, Si) ceramics at 673 K in air are shown in Fig. 3. The grain and grain boundary semicircular arcs of $Nd_{10}Si_5MgO_{26}$ and $Nd_{10}Si_5AlO_{26.5}$ are conspicuously smaller than those of undoped $Nd_{10}Si_6O_{27}$, which indicates that doping with

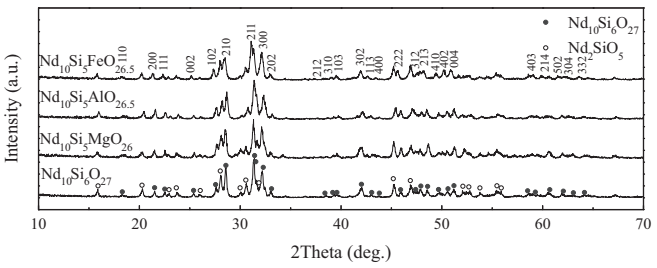

Fig. 1. XRD patterns of $Nd_{10}Si_5BO_{27-\delta}$ (B=Mg, Al, Fe, Si) ceramics sintered at 1923 K for 10 h.

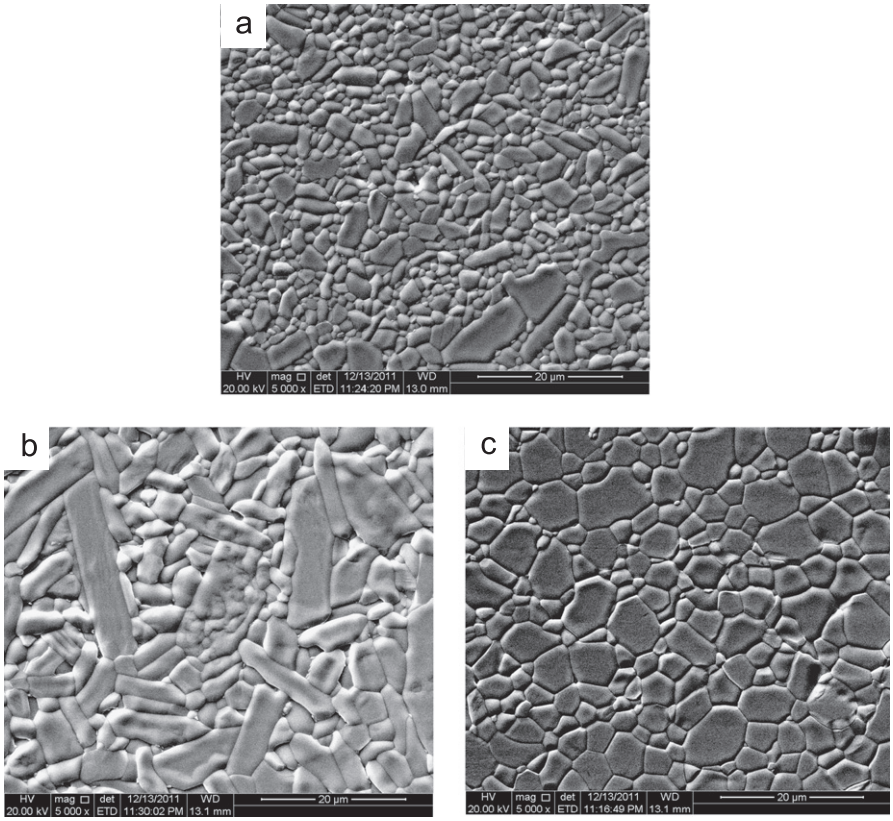

Fig. 2. Microstructure of $Nd_{10}Si_5BO_{27-\delta}$ (B=Al, Fe, Si) ceramics: (a) B=Al, (b) B=Fe, and (c) B=Si.

Table 1
Lattice parameters of $Nd_{10}Si_5BO_{27-\delta}$ (B=Mg, Al, Fe, Si) ceramics sintered at 1923 K for 10 h.

Materials	Lattice parameters (Å)		V (Å)^3
	a	c	
$Nd_{10}Si_6O_{27}$	9.632	6.802	546.447
$Nd_{10}Si_5MgO_{26}$	9.621	6.814	546.148
$Nd_{10}Si_5AlO_{26.5}$	9.626	6.819	547.173
$Nd_{10}Si_5FeO_{26.5}$	9.682	6.859	556.868

Mg^{2+} or Al^{3+} cations at the Si site can significantly reduce the grain and grain boundary resistance at 673 K.

In agreement with the fitted results, a series of capacitance values of different frequency semicircular arcs are shown in Table 3. The corresponding grain resistance (R_g) and grain boundary resistance (R_{gb}) are obtained from the fitting lines. R_g and R_{gb} are identified by the intercepts of high frequency semicircles and medium frequency semicircles on the Z' axes, respectively. Total conductivity of $Nd_{10}Si_5BO_{27-\delta}$ (B=Mg, Al, Fe, Si) ceramics at different temperatures is obtained from the following equation

$$\sigma = h/RS \tag{1}$$

where h is the thickness of specimen, S is the electrode area of the specimen surface, R is the total resistance, which includes R_g and R_{gb}. The total conductivity of each composition can be calculated in this way. The temperature dependence of total conductivity for each composition is analyzed from the following Arrhenius equation

$$\sigma T = \sigma_0 \exp\left(-E/k_B T\right) \tag{2}$$

where σ is the total conductivity, σ_0 is the pre-exponential factor related to the effective number of mobile oxide-ions, E is the activation energy for the electrical conduction process, k_B is the Boltzmann constant, and T is the absolute temperature. Fig. 3 presents the Arrhenius plots of total conductivity of $Nd_{10}Si_5BO_{27-\delta}$ (B=Mg, Al, Fe, Si) ceramics. The diffusion process of oxide-ions is thermally activated because the straight lines are well fitted to the Arrhenius relation. E and σ_0 can be calculated from the slope and the intercept of the linear fits in the Arrhenius plots for each composition, respectively. Activation energy E and pre-exponential factor σ_0 of total conductivity for $Nd_{10}Si_5BO_{27-\delta}$ (B=Mg, Al, Fe, Si) ceramics are shown

Table 2
Bulk densities of $Nd_{10}Si_5BO_{27-\delta}$ (B=Mg, Al, Fe, Si) ceramics sintered at 1923 K for 10 h.

Materials	Density (g cm^{-3})
$Nd_{10}Si_6O_{27}$	5.069
$Nd_{10}Si_5MgO_{26}$	5.168
$Nd_{10}Si_5AlO_{26.5}$	5.153
$Nd_{10}Si_5FeO_{26.5}$	5.299

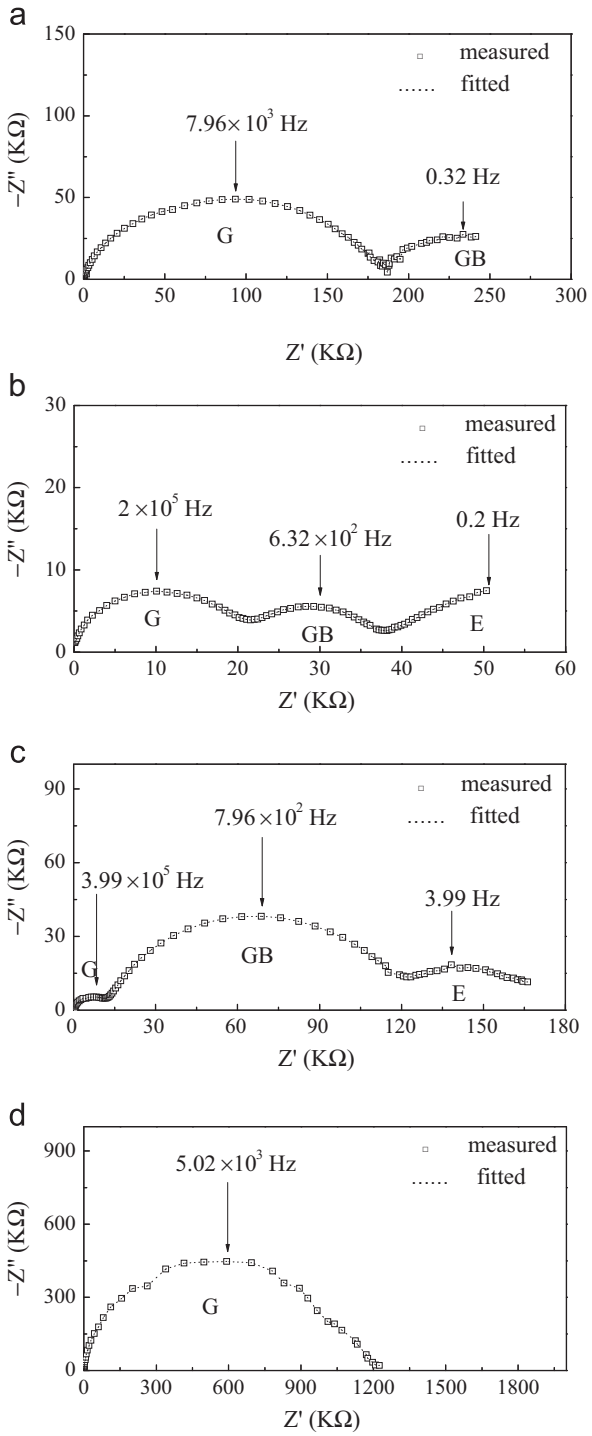

Fig. 3. Typical complex impedance plots of $Nd_{10}Si_5BO_{27-\delta}$ (B=Mg, Al, Fe, Si) ceramics at 673 K in air: (a) B=Si, (b) B=Mg, (c) B=Al, and (d) B=Fe. The grain (G), grain boundary (GB), and electrode (E) contributions are also indicated.

in Table 4. It can be seen that activation energies of $Nd_{10}Si_5BO_{27-\delta}$ (B=Mg, Al, Fe) ceramics are higher than that of $Nd_{10}Si_6O_{27}$ ceramic.

As evident from Fig. 4, doping with Mg^{2+} or Al^{3+} cations at the Si site leads to an enhanced total conductivity as contrasted with undoped $Nd_{10}Si_6O_{27}$ ceramic at all temperature levels, but doping with Fe^{3+} cation at the Si site has

Table 3
Fitting parameters of the $Nd_{10}Si_5BO_{27-\delta}$ (B=Mg, Al, Fe, Si) ceramics at 673 K.

Materials	R_g (Ω)	R_{gb} (Ω)	CPE_g (F)	CPE_{gb} (F)
$Nd_{10}Si_6O_{27}$	181,620	106,050	4.801×10^{-9}	6.4269×10^{-6}
$Nd_{10}Si_5MgO_{26}$	20,950	15,695	1.511×10^{-9}	1.6378×10^{-7}
$Nd_{10}Si_5AlO_{26.5}$	11,585	106,680	1.586×10^{-10}	1.1552×10^{-8}
$Nd_{10}Si_5FeO_{26.5}$	1,061,500	–	6.453×10^{-11}	–

R_g—grain resistance; CPE_g—high frequency semicircle constant phase element; R_{gb}—grain boundary resistance; CPE_{gb}—intermediate frequency semicircle constant phase element.

Table 4
Activation energy and pre-exponential factor of total conductivity for $Nd_{10}Si_5BO_{27-\delta}$ (B=Mg, Al, Fe, Si) ceramics.

Materials	Total conductivity	
	Activation energy (eV)	Pre-exponential factor (S K cm^{-1})
$Nd_{10}Si_6O_{27}$	0.80	6.02×10^2
$Nd_{10}Si_5MgO_{26}$	0.90	2.31×10^4
$Nd_{10}Si_5AlO_{26.5}$	1.07	1.88×10^5
$Nd_{10}Si_5FeO_{26.5}$	1.25	3.00×10^5

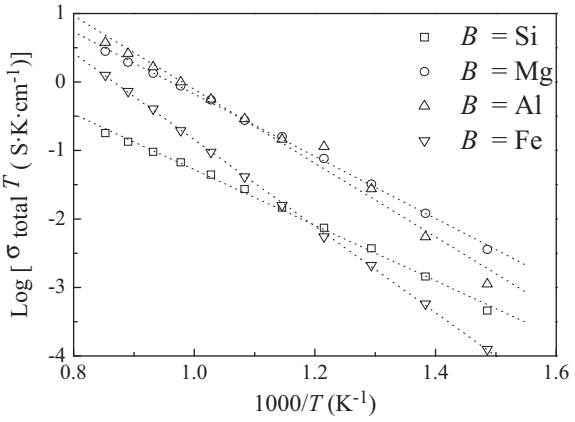

Fig. 4. Arrhenius plots of total conductivity of $Nd_{10}Si_5BO_{27-\delta}$ (B=Mg, Al, Fe, Si) ceramics.

only a little effect on improving the total conductivity above 873 K. Fig. 4 shows the highest total conductivity of 4.19×10^{-5} S cm^{-1} for $Nd_{10}Si_5MgO_{26}$ ceramic at 773 K, however, at 1073 K, $Nd_{10}Si_5AlO_{26.5}$ silicate has a total conductivity of 1.55×10^{-3} S cm^{-1}, which is two orders of magnitude higher than that of undoped $Nd_{10}Si_6O_{27}$, and is comparable to the value of $La_{10}Si_6O_{27}$ (5.84×10^{-3} S cm^{-1}) ceramic [16]. Total conductivity of $Nd_{10}Si_5BO_{27-\delta}$ (B=Mg, Al, Fe, Si) ceramics sintered at 1923 K for 10 h is given in Table 5. In the apatite-type silicates of $Ln_{10}(SiO_4)_6O_3$ (Ln=trivalent rare-earth elements), the structure is built up of isolated SiO_4 tetrahedra with excess oxide-ions, which are confirmed to migrate in the conduction channel by a complex sinusoidal pathway along the c-axis [4]. From Table 1,

Table 5
Total conductivity of $Nd_{10}Si_5BO_{27-\delta}$ (B=Mg, Al, Fe, Si) ceramics sintered at 1923 K for 10 h.

Materials	Total conductivity (S cm^{-1})	
	773 (K)	1073 (K)
$Nd_{10}Si_6O_{27}$	4.81×10^{-6}	8.90×10^{-5}
$Nd_{10}Si_5MgO_{26}$	4.19×10^{-5}	1.25×10^{-3}
$Nd_{10}Si_5AlO_{26.5}$	3.56×10^{-5}	1.55×10^{-3}
$Nd_{10}Si_5FeO_{26.5}$	2.73×10^{-6}	3.80×10^{-4}

doping with Mg^{2+} and Al^{3+} to the Si site in $Nd_{10}Si_5BO_{27-\delta}$ does not cause a distinct change in the cell volume due to similar lattice parameters of a and c as compared with $Nd_{10}Si_6O_{27}$ ceramic. However, doping with Fe^{3+} to the Si site leads to a very significant expansion in the cell volume. This indicates that the Fe^{3+} substitution on the Si site partly expands the SiO_4 tetrahedra, which will reduce the spacing of channels between the SiO_4 tetrahedron and Nd^{3+} cations in the hexagonal apatite structure. However, the oxide-ion conductivity in a hexagonal apatite-type structure depends upon the diffusion of interstitial oxide-ions through oxygen vacancies and through these channels between the SiO_4 tetrahedron and Nd^{3+} cations. Therefore, the Fe^{3+} substitution on the Si site will reduce the diffusion rate of oxide-ions through these channels, and leads to the decrease in ionic conductivity as contrasted with those ceramics doped with Mg^{2+} and Al^{3+}. In addition, the substitution of Mg^{2+} and Al^{3+} to the Si site probably induces the formation of a variety of oxygen vacancies in the hexagonal apatite structure, which also expedite the diffusion process of oxide-ions [17,18].

4. Conclusions

Apatite-type $Nd_{10}Si_5BO_{27-\delta}$ (B=Mg, Al, Fe, Si) ceramics were prepared via the high-temperature solid state reaction route. All $Nd_{10}Si_5BO_{27-\delta}$ ceramics consist of a hexagonal apatite structure with a space group $P63/m$ and a small amount of second phase Nd_2SiO_5. Neodymium silicates doped with Mg^{2+} and Al^{3+} cations have a higher total conductivity than undoped neodymium silicates. The enhanced oxide-ion conductivity in a hexagonal apatite-type structure depends upon the diffusion of interstitial oxide-ions through oxygen vacancies induced by the Mg^{2+} or Al^{3+} substitution to the Si^{4+} site and through the channels between the SiO_4 tetrahedron and Nd^{3+} cations. At 773 K, the highest total conductivity is 4.19×10^{-5} S cm^{-1} for $Nd_{10}Si_5MgO_{26}$ ceramic. At 1073 K, $Nd_{10}Si_5AlO_{26.5}$ silicate has a total conductivity of 1.55×10^{-3} S cm^{-1}, which is two orders of magnitude higher than that of undoped $Nd_{10}Si_6O_{27}$.

Acknowledgment

This work was financially supported by the National Natural Science Foundation of China (NSFC, Grant nos. 50972030, 51021002 and 51272054), and the Fundamental Research Funds for the Central Universities (Grant no. HIT.BRET1.2010006).

References

[1] C.H. Li, S.H. Hu, K.W. Tay, Y.P. Fu, Electrochemical characterization of gradient $Sm_{0.5}Sr_{0.5}CoO_{3-\delta}$ cathodes on $Ce_{0.8}Sm_{0.2}O_{1.9}$ electrolytes for solid oxide fuel cells, Ceramics International 38 (2012) 1557–1562.
[2] J. Choi, J. Im, I. Park, D. Shin, Preparation and characteristics of $Ba_{0.5}Sr_{0.5}Co_{0.8}Fe_{0.2}O_{3-\delta}$ cathodes for IT-SOFCs by electrostatic slurry spray deposition, Ceramics International 38S (2012) S489–S492.
[3] S. Nakayama, T. Kageyama, H. Aono, Y. Sadaoka, Ionic conductivity of lanthanoid silicates, $Ln_{10}(SiO_4)_6O_3$, (Ln=La, Nd, Sm, Gd, Dy, Y, Ho, Er and Yb), Journal of Materials Chemistry 5 (1995) 1801–1805.
[4] B. Li, W. Liu, W. Pan, Synthesis and electrical properties of apatite-type $La_{10}Si_6O_{27}$, Journal of Power Sources 195 (2010) 2196–2201.
[5] M. Higuchi, Y. Masubuchi, S. Nakayama, S. Kikkawa, K. Kodaira, Single crystal growth and oxide ion conductivity of apatite-type rare-earth silicates, Solid State Ionics 174 (2004) 73–80.
[6] S. Nakayama, M. Sakamoto, M. Higuchi, K. Kodaira, M. Sato, S. Kakita, T. Suzuki, K. Itoh, Oxide ionic conductivity of apatite type $Nd_{9.33}(SiO_4)_6O_2$ single crystal, Journal of the European Ceramic Society 19 (1999) 507–510.
[7] T. Nakao, A. Mineshige, Y. Ohnishi, M. Kobune, T. Yazawa, H. Yoshioka, Ionic and electronic conductivities for $Ln_{9.33+x}Si_6O_{26+1.5x}$ under various conditions, ECS Transactions 13 (2008) 39–45.
[8] E. Kendrick, J. Kendrick, A. Orera, P. Panchmatia, M.S. Islam, P.R. Slater, Novel aspects of the conduction mechanisms of electrolytes containing tetrahedral moieties, Fuel Cells 11 (2011) 38–43.
[9] E.V. Tsipis, V.V. Kharton, J.R. Frade, Electrochemical behavior of mixed-conducting oxide cathodes in contact with apatite-type $La_{10}Si_5AlO_{26.5}$ electrolyte, Electrochimica Acta 52 (2007) 4428–4435.
[10] M. Emirdag-Eanes, W.T. Pennington, J.W. Kolis, Synthesis, structural characterization, and magnetic properties of $NaRE_9(GeO_4)_6O_2$ (RE=Nd, Pr), Journal of Alloys and Compounds 366 (2004) 76–80.
[11] Y. Ohnishi, A. Mineshige, Y. Daiko, M. Kobune, H. Yoshioka, T. Yazawa, Effect of transition metal additives on electrical conductivity for La-excess-type lanthanum silicate, Solid State Ionics 181 (2010) 1697–1701.
[12] A. Orera, T. Baikie, P. Panchmatia, T.J. White, J. Hanna, M.E. Smith, M.S. Islam, E. Kendrick, P.R. Slater, Strategies for the optimisation of the oxide ion conductivities of apatite-type germanates, Fuel Cells 11 (2011) 10–16.
[13] Z.X. Qu, T.D. Sparks, W. Pan, D.R. Clarke, Thermal conductivity of the gadolinium calcium silicate apatites: effect of different point defect types, Acta Materialia 59 (2011) 3841–3850.
[14] I. Santacruz, J.M. Porras-Vazquez, E.R. Losilla, Preparation of aluminium lanthanum oxyapatite tapes, $La_{10}AlSi_5O_{26.5}$, by tape casting and reaction sintering, Journal of the European Ceramic Society 31 (2011) 1573–1580.
[15] S. Beaudet-Savignat, A. Vincent, S. Lambert, F. Gervais, Oxide ion conduction in Ba, Ca and Sr doped apatite-type lanthanum silicates, Journal of Materials Chemistry 17 (2007) 2078–2087.
[16] J. Xiang, Z.G. Liu, J.H. Ouyang, F.Y. Yan, Synthesis, structure and electrical Properties of rare-earth doped apatite-type lanthanum silicates, Electrochimica Acta 65 (2012) 561–565.
[17] Y.V. Pivak, V.V. Kharton, A.A. Yaremchenko, S.O. Yakovlev, A.V. Kovalevsky, J.R. Frade, F.M.B. Marques, Phase relationships and transport in Ti-, Ce- and Zr-substituted lanthanum silicate systems, Journal of the European Ceramic Society 27 (2007) 2445–2454.
[18] J. Xiang, Z.G. Liu, J.H. Ouyang, Y. Zhou, F.Y. Yan, Synthesis and electrical conductivity of $La_{10}Si_{5.5}B_{0.5}O_{27+\delta}$ (B=In, Si, Sn, Nb) ceramics, Solid State Ionics 220 (2012) 7–11.